The induced magnetosphere of Mars. Asymmetrical topology of the magnetic field lines

Edouard Dubinin, Ronan Modolo, Markus Fraenz, Martin Pätzold, Joachim Woch, Lihui Chai, Yong Wei, John E. P. Connerney, Jim Mcfadden, Gina Dibraccio, et al.

Geophysical Research Letters

RESEARCH LETTER
10.1029/2019GL084387

The Induced Magnetosphere of Mars: Asymmetrical Topology of the Magnetic Field Lines

E. Dubinin[1], R. Modolo[2], M. Fraenz[1], M. Päetzold[3], J. Woch[1], L. Chai[4], Y. Wei[4], J. E. P. Connerney[5], J. Mcfadden[6], G. DiBraccio[5], J. Espley[5], E. Grigorenko[7], and L. Zelenyi[7]

[1]Max-Planck-Institute for Solar System Research, Göttingen, Germany, [2]LATMOS/IPSL, UVSQ Universite, Paris-Saclay, UPMC University Paris CNRS, Guyancourt, France, [3]Abteilung Planetforschung, Rheinisches Institut fuer Umweltforschung, Cologne, Germany, [4]Key Lab of Earth and Planetary Physics, Institute of Geology and Geophysics, Beijing, China, [5]NASA Goddard Space Flight Center, Greenbelt, MD, USA, [6]Space Sciences Laboratory, University of California, Berkeley, CA, USA, [7]Institute of Space Research, Moscow, Russia

Key Points:
- Additional draping of the field lines in the opposite direction to the motional electric field appears
- Ion trail that contains dense and slowly moving tailward plasma arises
- Wrapping of the field lines is accompanied by the formation of loops of closed field lines and plasma vortices

Correspondence to:
E. Dubinin,
dubinin@mps.mpg.de

Citation:
Dubinin, E., Modolo, R., Fraenz, M., Pätzold, M., Woch, J., Chai, L., et al. (2019). The induced magnetosphere of Mars: Asymmetrical topology of the magnetic field lines. *Geophysical Research Letters*, *46*, 12,722–12,730. https://doi.org/10.1029/2019GL084387

Received 3 JUL 2019
Accepted 14 OCT 2019
Accepted article online 16 OCT 2019
Published online 27 NOV 2019

Abstract An asymmetrical pileup of the interplanetary magnetic field leads to an additional draping of the field lines in the opposite direction to the motional electric field. Such a draping and the associated magnetic field forces push the ionosphere plasma in the transverse direction opening a passage for an ion trail which contains dense and slowly moving plasma. We found that wrapping of the field lines around Mars starts in the hemisphere pointing in the direction of the motional electric field and propagates to the opposite hemisphere where the cross-flow component of the draped interplanetary magnetic field changes sign in a broad area accompanied by the formation of loops of closed field lines. Reconnection near Mars accompanied by the generation of plasma vortices imposes serious constraints on the ion dynamics and their escape through the tail. The existence of all these features is confirmed by hybrid simulations.

1. Introduction

The interaction of solar wind with Mars starts at large distances from the planet because of the extended hydrogen exosphere and hot oxygen corona. After being ionized by solar irradiance, and charge-exchange with neutrals, hydrogen and oxygen atoms are picked up by the solar wind. Because of the small size of Mars as compared to the oxygen cyclotron-radius, oxygen ions are deflected and accelerated toward the hemisphere in which the solar wind motional electric field is pointing away from Mars (E^+ hemisphere), producing a strong asymmetry in the global interaction pattern at the dayside. This ion motion provides an excess of transverse momentum in the system, which must be balanced by the motion of the solar wind protons in the opposite direction. A small lateral deviation of the solar wind velocity (~5 km/s) in the direction opposite to the direction of the motional electric field indicating a weak mass-loading effect is observed even upstream of the bow shock (Halekas et al., 2017). Closer to Mars the number density of oxygen ions grows and mass-loading effects manifesting in the solar wind deflection become more pronounced. Nevertheless, there is still a generally rather symmetric deflection of the plasma flow around the planetary obstacle (Dubinin et al., 2018). Approaching further to Mars, the solar wind interacts with the ionosphere and the crustal fields, which produces a rather intricate topology of the magnetic field. To separate the features of the draping and crustal components working in different coordinate systems occurs useful (DiBraccio et al., 2018; Dubinin & Fraenz, 2015; Dubinin et al., 2017; Yeroshenko et al., 1990). Since the orientation of the interplanetary magnetic field (IMF) and the motional electric field varies with time, the relevant coordinate system for the description of the induced draping magnetosphere is the Mars Solar Electric system, which has the X_{MSE} axis antiparallel to the upstream solar wind flow, the Y_{MSE} axis along the cross-flow magnetic field component of the IMF in the solar wind, and the Z_{MSE} axis pointing in the direction of the solar wind motional electric field ($-V_{sw} \times B_{IMF}$), where V_{sw} and B_{IMF} are the vectors of the velocity and the magnetic field in the solar wind, respectively. When we rotate the spacecraft trajectories into MSE coordinates and apply temporal averaging the effects of the crustal magnetic field on an asymmetry are almost cancelled out. In MSE coordinates the distribution of the external magnetic field around Mars becomes well organized and an asymmetry of oxygen ion fluxes caused by the motional electric field is well visible (Dubinin et al., 2011; Dong et al., 2015). In this paper we analyze the main features of the induced component, and therefore, we

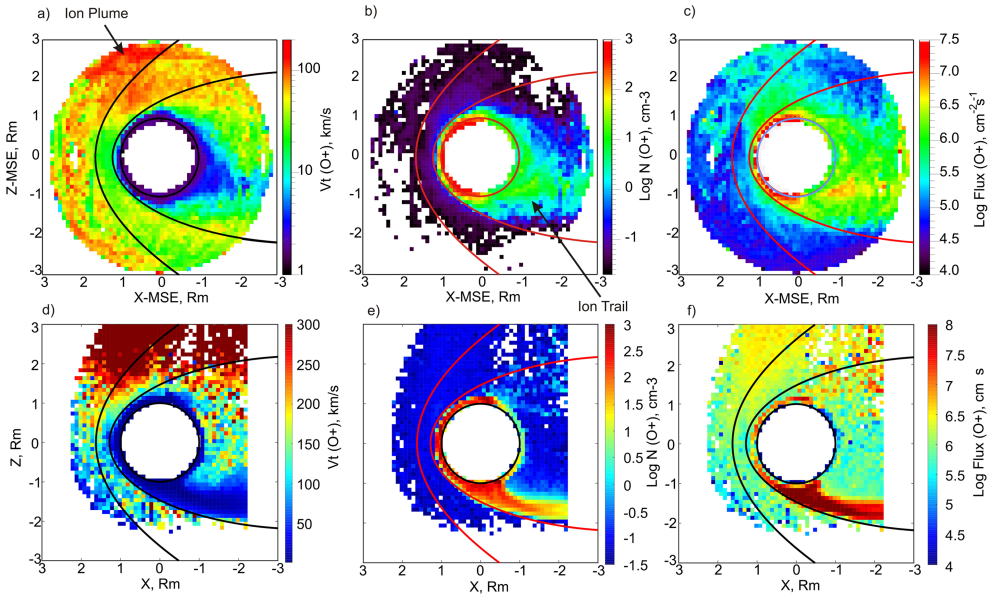

Figure 1. Maps of the O^+ ion velocity (a), density (b), and fluxes (c) plotted in the XZ_{MSE} planes ($-0.5R_M < Y_{\mathrm{MSE}} < 0.5R_M$). Black (red) curves show the nominal positions of the bow shock and the magnetospheric boundary (Dubinin et al., 2006). (d–f) Maps of the same values from the simulation run. Ion plume and ion trail are well seen in the observations and simulations. MSE = Mars Solar Electric system.

use MSE coordinates and constrain ourselves to the measurements made only in the northern hemisphere of Mars in which the role of the crustal field is much weaker. We investigate how the asymmetry that is related with the motional electric field propagates to the tail. Note that different features of asymmetry of the Martian magnetosphere were discussed in Inui et al. (2019), Dong et al. (2015), Dubinin et al. (2011), Chai et al. (2019), Harada et al. (2015), and Modolo et al. (2016). Focus of this paper is close integration of the Mars Atmosphere and Volatile EvolutioN (MAVEN) observations, hybrid simulations, and physical interpretation.

2. Observations and Simulations

We present observations carried out by the MAVEN spacecraft between 1 November 2014 and 15 August 2017. MAVEN was inserted into an elliptical orbit with periapsis and apoapsis of 150 and 6,200 km, respectively, and with a period of 4.5 hr (Jakosky et al., 2015). We utilize the magnetic field data from two independent triaxial fluxgate magnetometers mounted on the booms of the MAVEN spacecraft (Connerney, Espley, Lawton, et al., 2015; Connerney, Espley, DiBraccio, et al., 2015). Plasma parameters are measured by the Supra-Thermal And Thermal Ion Composition instrument, which gauges the ion composition and energy spectra of ion fluxes in the range of 0.1 eV to 30 keV (McFadden et al., 2015). The spacecraft velocity and potential were used calculating the moments of the ion distribution functions. We utilize the IMF orientation on each MAVEN orbit by averaging the magnetometer data in the upstream solar wind over 30 min. During the orbits when MAVEN was not in the solar wind, we use the magnetic field measurements in the magnetosheath. Note that for these cases the clock angle errors due to the IMF deformations may appear (Dong et al., 2019; Fang et al., 2018). We processed all orbits in order to study the global features of the Martian magnetosphere without any additional assumptions about the IMF orientation. The observations by MAVEN are complemented by hybrid simulations of the solar wind/Mars interaction where electrons are treated as a magnetized fluid and the ions are treated as single particles (see details in Modolo et al., 2016), which allow not only to switch off crustal sources but also to provide new details which may be missed in the averaged picture retrieved from the MAVEN data.

Figure 1 (top panels) shows the maps of the velocity (a), density (b), and fluxes (c) of oxygen ions in the XZ_{MSE} plane ($-0.5\ R_M < Y_{\mathrm{MSE}} < 0.5R_M$). Oxygen ions detected in the upstream region originate from the hot oxygen corona and are picked up by solar wind. A strong asymmetry between the upper E^+ and lower E^- hemispheres is observed. Ions with a higher speed form a plume in the E^+ magnetosheath and the adjacent

region in the solar wind (panel a). In contrast, an asymmetrical void of such ions is seen behind the planet. This trail, void of fast O^+ ions, is filled by a dense and slow ionospheric plasma shifting toward the E^- hemisphere (panel b). The highest fluxes of the escaping oxygen ions occur through this channel (panel c).

Most of the above features are also seen in the lower panels of Figure 1, which present similar maps of the velocity (d), density (e), and flux (f) of O^+ ions obtained from the simulations. The simulations with the spatial resolution of 50 km were done for a solar wind number density of 2.7 cm^{-3}, a velocity of 485 km/s, an IMF orientation (−1.6, 2.5, 0) nT, and without crustal field sources. The simulation run corresponds to the run named "RUN C" in Modolo et al. (2016) where a reader can find more details. Since the IMF lies in the XY plane and the B_y component is positive, MSO and MSE coordinates coincide in the simulations. The plume of oxygen ions with high speeds in the E^+ hemisphere and the trail of low-energy ions in the E^- hemisphere are clearly seen in the simulations too. Note that the trail in the simulations occurs more narrow as compared to the averaged picture obtained from the MAVEN observations. Different solar wind conditions and the IMF orientation might contribute to expansion of the ion trail in the averaged picture.

Figures 2a–2d show maps of the magnetic field projections onto the XZ planes taken at the different Y_{MSE} distances from the central plane. The maps only contain vectors within the nominal position of the boundary of the Martian magnetosphere. Color depicts the B_z component. For these and further plots we applied a more strict selection of the data points. To reduce the probability of errors related with the selection of the MSE coordinates, we selected only orbits with $B_x > 0$ at $Y_{\mathrm{MSE}} < 0$ and with $B_x < 0$ at $Y_{\mathrm{MSE}} > 0$, respectively. This selection also removes the twisting effects of the current sheet (Dubinin et al., 2017; DiBraccio et al., 2018). In the cross sections taken at $Y = [0.1, 0.3]R_M$ and $Y = [-0.1, -0.3]R_M$ we observe that close to Mars the field line projections envelope the planet. With a distance from Mars the region with the negative values of the B_z component at $Y_{MSE} > 0$, seen as pink/purple bins in panel (a), expands from the E^+ to E^- hemisphere. Similarly, the region with positive values of the B_z component (green bins) at $Y_{\mathrm{MSE}} < 0$ also spreads to the E^- hemisphere. With a distance from the central plane ($Y_{\mathrm{MSE}} = 0$; panels c and d) this asymmetry in the field geometry enhances. It is well seen in panels (e)–(h) of Figure 2, which present maps of the magnetic field projections onto the YZ_{MSE} planes at the different distances from Mars. It is observed that asymmetry in the field topology between the both hemispheres appearing already at the dayside becomes obvious at the nightside. A strong transverse bending of field lines associated with a draping in the direction opposite to the direction of the motional electric field is seen. This bending gradually decreases with the distance to Mars but persists down to $X \sim -2.5R_M$. Another interesting feature is a change of sign of the cross-flow $B_{y-\mathrm{MSE}}$ component of the magnetic field in the E^- hemisphere that is well seen closer to Mars (panel f). This gives the impression of the clockwise rotation of the magnetic field (Chai et al., 2019). A change of sign of the B_y component corresponds to a wrapping of the field lines around Mars.

Figure 3a shows a map of the projections of the magnetic field onto the YZ_{MSE} plane ($X_{\mathrm{MSE}} = -2R_M$) obtained from the hybrid simulations. Here we have a slightly different inputs as compared to the "RUN C" (Figures 1d–1f). The solar wind density and velocity are 4.7 cm^{-3} and 450 km/s, respectively. The IMF has the only the B_y component (4 nT) to get symmetrical tail lobes with a plane current sheet. Color depicts the B_x component of the magnetic field. Here we observe some new features probably missed in the averaged picture obtained from the observations. Besides the clockwise rotation of the B_{yz} vector in the center of the tail ($r <\sim 1R_M$) caused by draping features in the transverse direction and a reversal of the B_y component in the E^- hemisphere, described by as a "looping" by Chai et al. (2019), we also observe that signatures of Hall currents are appearing in the thin central current sheet at $Z \sim 1$–$1.3\ R_M$ (Figure 3b). Similar magnetic field perturbations caused by Hall currents were observed by Halekas et al. (2009) and Harada et al. (2017). A plane geometry of the central current sheet is destroyed at $Z \leq 0$ with a reversal of the B_y component indicating a probable disruption of the current sheet by the reconnection.

Figure 4 compares maps of the B_y component of the magnetic field and the density of O^+ ions in the XY_{MSE} planes at the different Z_{MSE} distances. The two upper (lower) panels correspond to the measurements in the E^+ (E^-) hemisphere, respectively. Wrapping of the magnetic field lines becomes visible already in the E^+ hemisphere and gradually enhances toward the E^- hemisphere. Wrapping is closely related to the distribution of the ion density in the ionosphere at the nightside and in the ionospheric trail. With expansion of the ionosphere toward the E^- hemisphere magnetic field lines in the near Mars tail appear to be wrapped more tightly around the planet.

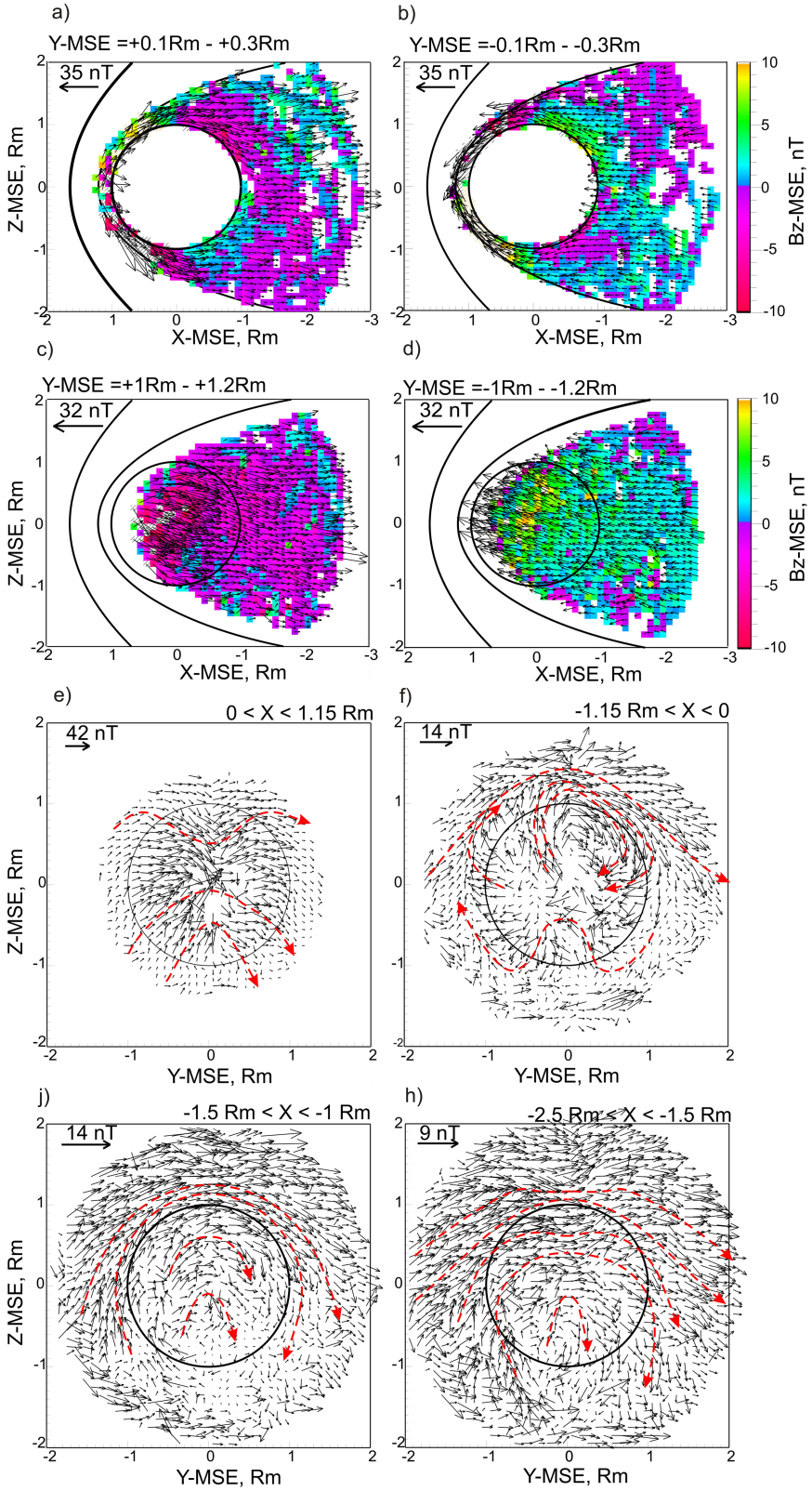

Figure 2. (a–d) Maps of the projections of the magnetic field onto the XZ_{MSE} plane at the different Y_{MSE} distances. Color shows the value of the $B_{z-\mathrm{MSE}}$ component. (e–h) Maps of the magnetic field projections onto the YZ planes taken at the different distances from Mars. Dashed lines approximately show the projections of the field lines. MSE = Mars Solar Electric system.

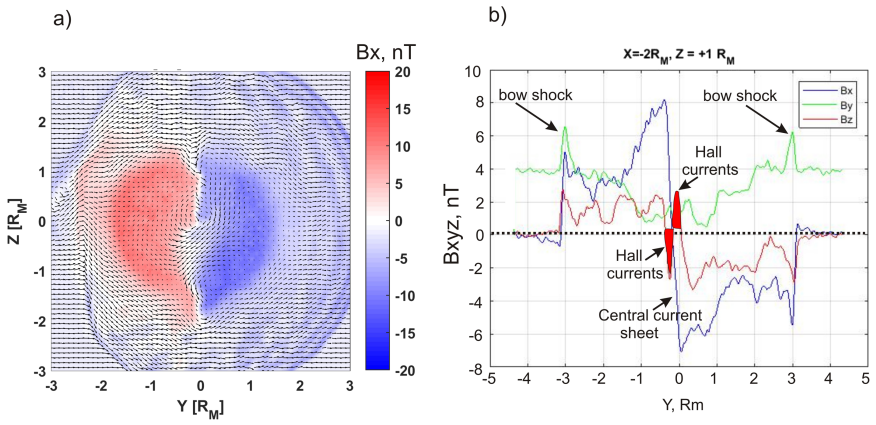

Figure 3. (a) Map of the projections of the magnetic field vectors onto the YZ_{MSE} plane in the Martian tail obtained in the hybrid simulations. Color shows the B_x component of the field. (b) Three components of the magnetic field along the Y axis at $Z = 1\ R_M$.

Figures 5a and 5b show maps of the projections of the magnetic field in the XY_{MSE} planes in the E^+ ($Z_{\mathrm{MSE}} = [0.9, 1.1]R_M$) and $E^-(Z_{\mathrm{MSE}} = [-0.9, -1.1]R_M)$ hemisphere, respectively. Color depicts the value of the B_y component of the field. Closed loops of the magnetic field lines appear in the E^- hemisphere while in the E^+ hemisphere we observe a classical draping configuration. Reconnection near Mars in the E^- hemisphere is accompanied by the generation of a plasma vortex identified by sunward ion motion. Figure 5e depicts a map of the velocity projections of the H^+ ions in the XY_{MSE} plane ($Z_{\mathrm{MSE}} = [-0.9, -1.1]R_M$). In the shaded black bins the ions have a velocity value of $|V| > 50$ km/s in the antisunward direction. A reversal of the flow occurs in the region of the closed magnetic field loop. A similar vortex appears in the motion of the O^+ ions too (not shown here). Figures 5c, 5d, and 5f depict maps of the magnetic field and the velocity of the planetary protons obtained by the hybrid simulations with the same input parameters as in Figure 3. In the E^+ hemisphere a common draping of the IMF over the ionosphere occurs. In the E^- hemisphere closed loops of the magnetic field lines appear, which can clearly be seen from the map of the magnetic field projections onto the XY_{MSE} plane at $Z_{\mathrm{MSE}} = -0.9 - 1.1R_M$ (Figure 5d). This feature of the field closure propagates far to the tail. Note that such configuration of the magnetic field is already observed at $Z_{\mathrm{MSE}} \leq 0$, where the B_y component changes sign (see Figure 3). The reversal of the magnetic field curvature is also accompanied by a reversal of the plasma flow (Figure 5f).

3. Discussion

Although the crustal magnetic field significantly complicates the field topology near the planet adding components typical for the magnetized planets, it is possible to highlight the main features of the induced magnetosphere by using MSE coordinates and MAVEN data for the northern hemisphere in which the role of crustal magnetization is less significant. It is shown that the flow pattern of planetary ions at Mars is very asymmetric. A shift of the ionosphere region which is populated by O^+ and O_2^+ ions to the $-Z_{\mathrm{MSE}}$ direction and the formation of the ion trail might be caused by similar processes which were widely discussed for the AMPTE artificial comet (see, e.g., Chapman, 1989; Haerendel et al., 1986; Harold & Hassam, 1994). The initial momentum of the solar wind is transferred into a compression of the magnetic field. The Hall current and large-scale deflection of the solar wind in the $V_{\mathrm{sw}} \times B$ direction brake the symmetry of the field pileup and cause an asymmetrical draping of the IMF lines around the ionospheric obstacle. This will shift the pileup region to the $-V_{\mathrm{sw}} \times B_{\mathrm{IMF}}$ side (E^+ hemisphere). The asymmetric field pileup causes the ionosphere to accelerate in the $V_{\mathrm{sw}} \times B_{\mathrm{IMF}}$ direction (E^- hemisphere). The magnetic pressure drives the ionosphere tailward and also in the transverse direction.

In addition to the classical tailward stretching of the field lines a draping in the direction opposite to the direction of the motional electric field in the solar wind appears. Due to the force experienced by the ionosphere in this direction the ionosphere shifts and becomes very asymmetrical. Fluxes of escaping ions in the tail turn out to be also very asymmetrical with the formation of the ion trail in the E^- hemisphere. The trail contains a dense and slowly moving plasma with higher fluxes than in the opposite E^+ hemisphere. Such an asymmetry of the flow pattern was also observed by Inui et al. (2019).

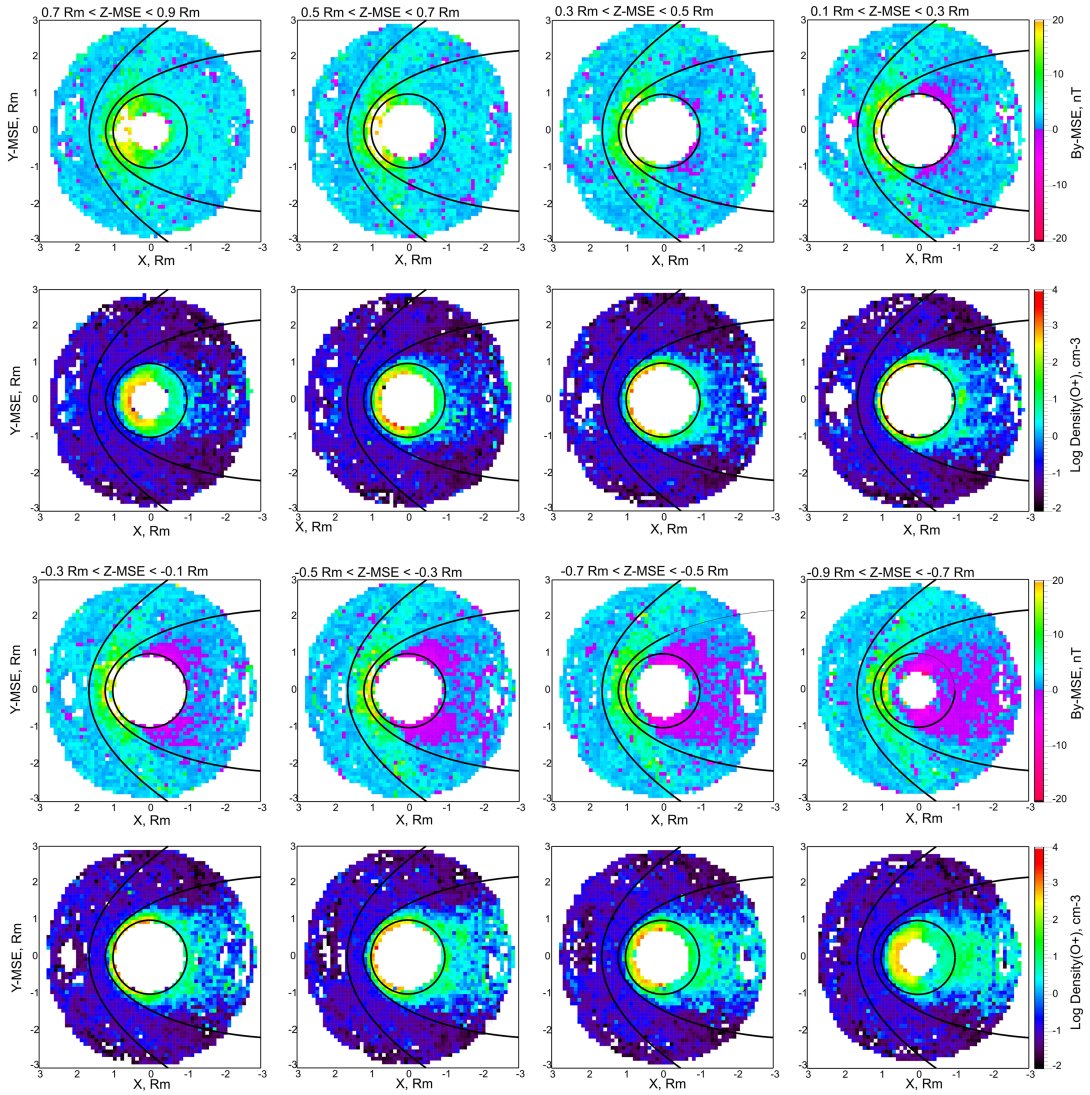

Figure 4. Maps of the B_y component of the magnetic field and the density of O^+ ions in the XY_{MSE} planes at the different Z_{MSE} positions. MSE = Mars Solar Electric system.

Closer to Mars we observe clear signatures of a reversal of the $B_{y-\mathrm{MSE}}$ component that creates the impression of a clockwise rotation of the magnetic field, which together with stretching of the field lines in the transverse direction explains the "looping" features discussed by Chai et al. (2019). Wrapping of the field lines around Mars starting in the E^+ hemisphere propagates to the E^- hemisphere where the cross-flow component of the draped IMF changes sign in a broadening area.

Wrapping is closely related to distribution of the plasma density. Because the thermal pressure in the upper ionosphere of Mars is generally weak as compared to the incident solar wind pressure, the IMF penetrates deep into the ionosphere which broadens the solar wind/ionosphere current system. The magnetic field lines, mainly horizontal in the ionosphere, encapsulate the ionospheric obstacle not only at the dayside but also at the nightside by a reversal of sign of the B_y component (see, e.g., Luhmann et al., 1981). Note that an asymmetrical wrapping of the magnetic field lines was also observed in the near Venus tail (Zhang et al., 2010).

We found that a part of the magnetic field flux generated by the toroidal pressure gradient current ($j \sim B \times \nabla P$) system is closed in the near Mars tail that leads to the formation of the loops with the closed field lines. The appearance of the closed field loops is able to stop the operation of the tailward "jet-engine" ion acceleration in the plasma sheet ($j \times B$) and to produce sunward fluxes of the ions similar as it happens during classical

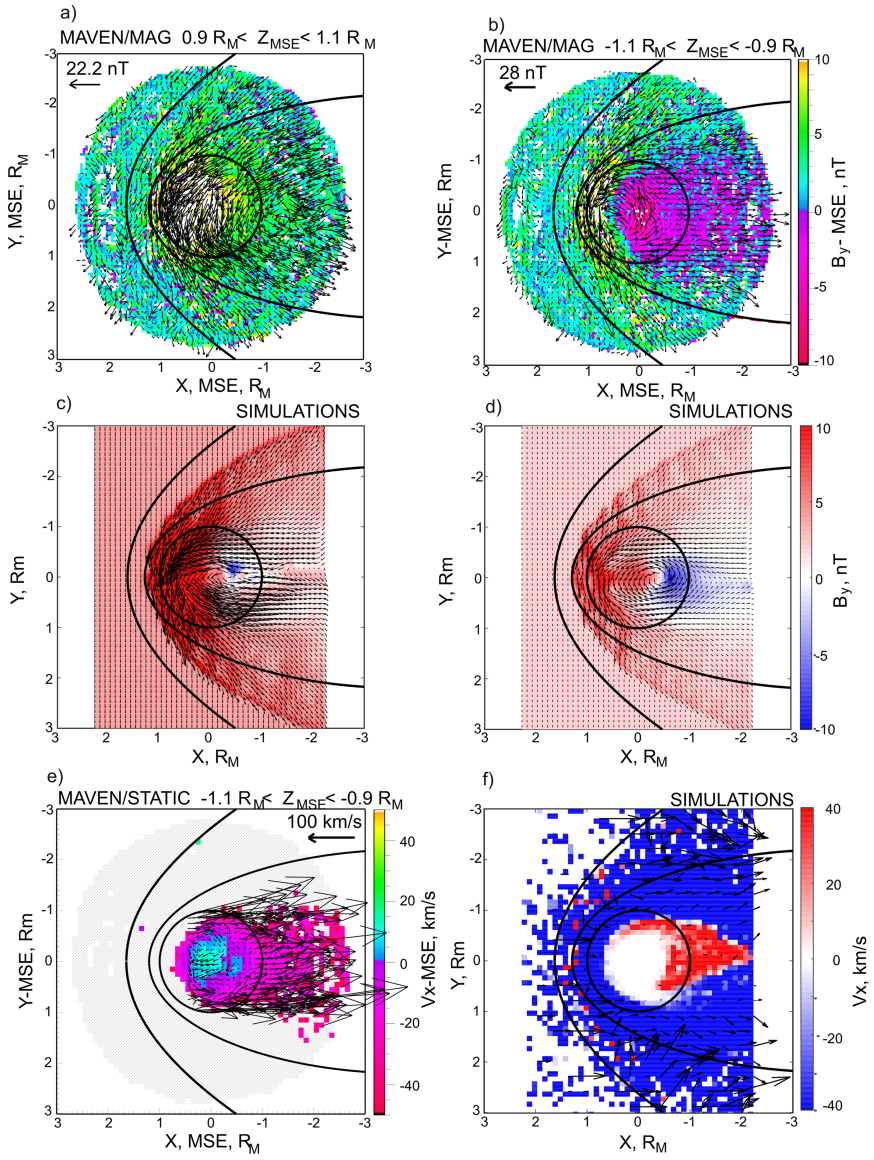

Figure 5. (a, b) Maps of the projections of the magnetic field onto the XY_{MSE} planes in the E^{+} and E^{-} hemispheres, respectively. Color shows the $B_{y-\mathrm{MSE}}$ component of the magnetic field. (c, d) Similar maps of the magnetic field obtained in the hybrid simulations. (e) Map of the velocity vectors of the protons observed in the XY_{MSE} plane at $Z_{\mathrm{MSE}} = [-0.9, -1.1]R_M$. Color shows the value of the V_x velocity. (f) Map of the proton velocity vectors obtained in the hybrid simulations. Color shows the value of the V_x velocity. MSE = Mars Solar Electric system; MAVEN = Mars Atmosphere and Volatile EvolutioN.

reconnection. Although the existence of the closed loops seen in the field projections does not unquestioningly imply a closure of the field lines, the observations by Harada et al. (2015, 2017) of reconnection signatures with preferentially sunward ion fluxes and of the trapped electrons with two-sided loss cones in the E^{-} hemisphere support the idea of a closed field line topology. These signatures were observed approximately in the same region where we see the closed loops, and they are not correlated with local crustal field sources. Hara et al. (2017) have also observed an asymmetry of the ion fluxes toward the planet with their dominance in the E^{-} hemisphere. Additional evidence for the closed field line topology was found by Xu et al. (2017). Figure 6 shows a sketch illustrating the main features of the induced magnetosphere of Mars. The gradient of the magnetic pressure and the magnetic field tensions arising due to bending of the field lines in the E^{+} hemisphere, push the ionospheric plasma in the direction opposite to the direction of the motional electric field. Under action of this force and the force in the tailward direction the ion trail is formed in the E^{-} tail. A shift of the ionosphere is accompanied by a strong wrapping of the magnetic field lines and

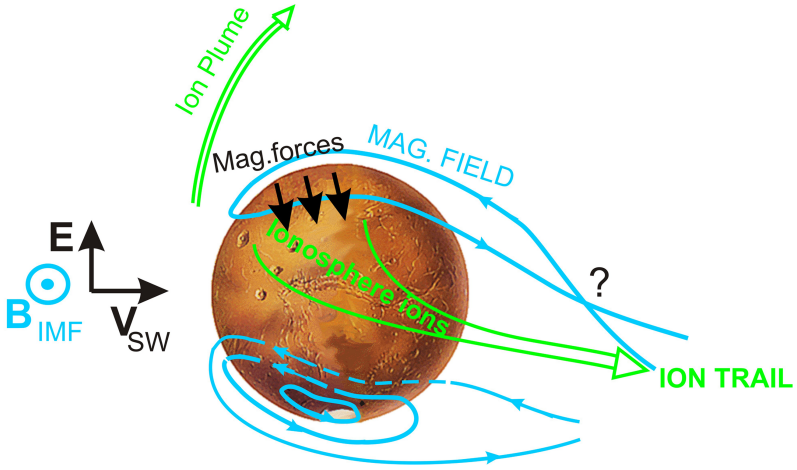

Figure 6. Sketch of the magnetic field topology in the E^+ and E^- hemispheres. A closed field configuration arises in the E^- hemisphere. According to the hybrid simulations (see also Chai et al., 2019), the field lines passing Mars in the E^+ hemisphere can also reconnect with the formation of the closed loops.

their closure in the near Mars tail. We have shown that the above characteristics are also observed in the global hybrid simulations made without the crustal magnetic sources. The simulations show that a closure of the field lines can occur in wider and distant areas. The important feature is the reversal of plasma flows in these regions. Note that a similar asymmetry in the flow pattern and the magnetic field is also observed in the near Venus tail (Chai et al., 2016; Dubinin et al., 2013, 2017). The hybrid simulations show that a reversal of the plasma flow and the field reconfiguration are the typical features, which can significantly change the conventional wisdom on the symmetrical structure and dynamics of the induced magnetosphere. The observations and simulations also raise a lot of questions about the reconnection processes in the induced magnetospheres and their role in ion losses through the tail. In particular, explanation for the differences in the reconnection areas between the simulations and the averaged picture retrieved from the observations is yet to be provided. Mechanism responsible for disruption of the tail current sheet and reconnection remains unknown. Another interesting question is how fast the asymmetries in the field topology and ion fluxes in the tail response to changes in the IMF. In future work we will address these questions.

Acknowledgments
The MAVEN project is supported by NASA through the Mars Exploration Program. MAVEN data are publicly available through the Planetary Data System. Authors E. D. and M. P. wish to acknowledge support from DFG for supporting this work by Grant PA 525/14-1. Authors E. D. and M. F. wish to acknowledge support from DLR by Grant 50QM1703.

References

Chai, L., Wan, W., Wei, Y., Zhang, T., Exner, W., Fraenz, M., et al. (2019). The induced global looping magnetic field on Mars. *The Astrophys Journal Letters*, *L27*(7pp), 871. https://doi.org/10.3847/2041-8213/aaff6e

Chapman, S. (1989). On the bulk motion of the ion clouds formed by the AMPTE solar wind/magnetosheath releases. *Journal of Geophysical Research*, *94*, 227–240.

Chai, L., Wei, Y., Wan, W., Zhang, T., Rong, Z., Fraenz, M., Dubinin, E., Zhang, H., Zhong, J., Han, X., & Barabash, S. (2016). An induced global magnetic field looping around the magnetotail of Venus. *Journal of Geophysical Research: Space Physics*, *121*, 688–698. https://doi.org/10.1002/2015JA021904

Connerney, J. E. P., Espley, J., DiBraccio, G. A., Gruesbeck, J. R., Oliversen, R. J., Mitchell, D. L., et al. (2015). First results of the magnetic field investigation. *Geophysical Research Letters*, *42*, 8819–8827. https://doi.org/10.1002/2015GL065366

Connerney, J. E., Espley, J., Lawton, P., Murphy, S., Odom, J., Oliversen, R., & Sheppard, D. (2015). The MAVEN magnetic field investigation. *Space Science Reviews*, *195*(1-4), 257–291. https://doi.org/10.1007/s11214-015-0169-4

DiBraccio, G. A., Luhmann, J. G., Curry, S. M., Espley, J. R., Xu, S., Mitchell, D. L., et al. (2018). The twisted configuration of the Martian magnetotail: MAVEN observations. *Geophysical Research Letters*, *45*, 4559–4568. https://doi.org/10.1029/2018GL077251

Dong, Y., Fang, X., Brain, D. A., Hurley, D. M., Halekas, J. S., Espley, J. R., et al. (2019). Magnetic field in the Martian magnetosheath and the application as an IMF clock angle proxy. *Journal of Geophysical Research: Space Physics*, *124*, 4295–4313. https://doi.org/10.1029/2019JA026522

Dong, Y., Fang, X., Brain, D. A., McFadden, J. P., Halekas, J. S., Connerney, J. E., et al. (2015). Strong plume fluxes at Mars observed by MAVEN: An important planetary ion escape channel. *Geophysical Research Letters*, *42*, 8942–8950. https://doi.org/10.1002/2015GL065346

Dubinin, E., & Fraenz, M. (2015). Magnetotails of Mars and Venus. In A. Keiling, C. M. Jackman, & P. A. Delamere (Eds.), *Magnetotails in the solar system* (pp. 43–59). Hoboken, NJ: John Wiley. https://doi.org/10.1002/9781118842324.ch3

Dubinin, E., Fraenz, M., Fedorov, A., Lundin, R., Edberg, N., Duru, F., & Vaisberg, O. (2011). Ion energization and escape on Mars and Venus. *Space Science Review*, *173-211*(2011), 162. https://doi.org/10.1007/s11214-011-9831-7

Dubinin, E., Fraenz, M., Pätzold, M., Halekas, J. S., Mcfadden, J., Connerney, J. E. P., et al. (2018). Solar wind deflection by mass loading in the Martian magnetosheath based on MAVEN observations. *Geophysical Research Letter*, *45*, 2574–2579. https://doi.org/10.1002/2017GL076813

Dubinin, E., Fraenz, M., Pätzold, M., McFadden, J., Halekas, J., DiBraccio, G., Connerney, J., Eparvier, F., Brain, D., Jakosky, B., Vaisberg, O., & Zelenyi, L. (2017). The effect of solar wind variations on the escape of oxygen ions from Mars through different channels: MAVEN observations. *Journal of Geophysical Research: Space Physics*, *122*, 11,285–11,301. https://doi.org/10.1002/2017JA024741

Dubinin, E., Fraenz, M., Zhang, T., Woch, J., Wei, Y., Fedorov, A., Barabash, S., & Lundin, R. (2013). Plasma in the near Venus tail: Venus express observations. *Journal of Geophysical Research: Space Physics*, *118*, 7624–7634. https://doi.org/10.1002/2013JA019164.210

Dubinin, E., Fraenz, M., Woch, J., Roussos, E., Barabash, S., Lundin, R., Winningham, J. D., Frahm, R. A., & Acuna, M. (2006). Plasma morphology at Mars. ASPERA-3 observations. ASPERA-3 observations. *Space Science Review*, *126*, 209–238. https://doi.org/10.1007/s11214-006-9039-4

Fang, X., Ma, Y., Luhmann, J., Dong, Y., Brain, D., Hurley, D., et al. (2018). The morphology of the solar wind magnetic field draping on the dayside of Mars and its variability. *Geophysical Research Letter*, *45*, 3356–365. https://doi.org/10.1002/2018GL077230

Haerendel, G., Paschmann, G., Baumjohann, W., & Carlson, C. W. (1986). Dynamics of the artificial AMPTE comet. *Nature*, *320*, 24.

Halekas, J. S., Eastwood, J. P., Brain, D. A., Phan, T. D., Øieroset, M., & Lin, R. P. (2009). In situ observations of reconnection Hall magnetic fields at Mars: Evidence for ion diffusion region encounters. *Journal Geophysical Research*, *114*, A11204. https://doi.org/10.1029/2009JA014544

Halekas, J. S., Ruhunusiri, S., Harada, Y., Collinson, G., Mitchell, D. L., Mazelle, C., et al. (2017). Structure, dynamics, and seasonal variability of the Mars-solar wind interaction: MAVEN solar wind ion analyzer inflight performance and science results. *Journal Geophysical Research: Space Physics*, *121*, 547–578. https://doi.org/10.1002/2016JA023167

Hara, T., Luhmann, J. G., Leblanc, F., Curry, S. M., Seki, K., Brain, D. A., et al. (2017). MAVEN Observations on a hemispheric asymmetry of precipitating ions towards the Martian upper atmosphere according to the upstream solar wind electric field. *Journal Geophysical Research: Space Physics*, *122*, 1083–1101. https://doi.org/10.1002/2016JA023952

Harada, Y., Halekas, J. S., McFadden, J. P., Espley, J., DiBraccio, G. A., Mitchell, D. L., et al. (2017). Survey of magnetic reconnection signatures in the Martian magnetotail with MAVEN. *Journal Geophysical Research: Space Physics*, *122*, 5114–5131. https://doi.org/10.1002/2017JA023348

Harada, Y., Halekas, J. S., McFadden, J. P., Mitchell, D. L., Mazelle, C., Connerney, J. E. P., et al. (2015). Magnetic reconnection in the near-Mars tail: MAVEN observations. *Geophysical Research Letter*, *42*, 8838–8845. https://doi.org/10.1002/2015GL065004

Harold, J. B., & Hassam, A. B. (1994). Two ion fluid numerical investigations of solar wind gas releases. *Journal Geophysical Research*, *99*(A10), 19,325–19,340.

Inui, S., Seki, K., Sakai, S., Brain, D. A., Hara, T., McFadden, J. P., et al. (2019). Statistical study of heavy ion outflows from Mars observed in the Martian induced magnetotail by MAVEN. *Journal Geophysical Research: Space Physics*, *124*, 5482–5497. https://doi.org/10.1029/2018JA026452

Jakosky, B. M., Lin, R. P., Grebowsky, J. M., Luhmann, J. G., Mitchell, D. F., Beutelschies, G., et al. (2015). The Mars Atmosphere and Volatile Evolution (MAVEN) mission. *Space Science Review*, *195*(1-4), 3–48. https://doi.org/10.1007/s11214-015-0139-x

Luhmann, J. G., Elphic, R. C., Russell, C. T., Slavin, J. A., & Mihalov, J. D. (1981). Observations of large scale steady magnetic fields in the night-side Venus ionosphere and near wake. *Geophysical Research Letters*, *8*, 517–520. https://doi.org/10.1029/GL008i005p00517

McFadden, J. P., Kortmann, O., Curtis, D., Dalton, G., Johnson, G., Abiad, R., et al. (2015). MAVEN SupraThermal And Thermal Ion Compostion (STATIC) instrument. *Space Science Review*, *195*, 199–256. https://doi.org/10.1007/s11214-015-0175-6

Modolo, R., Hess, S., Mancini, M., Leblanc, F., Chaufray, J.-Y., Brain, D., et al. (2016). Mars-solar wind interaction: LatHyS, an improved parallel 3-D multispecies hybrid model. *Journal of Geophysical Research: Space Physics*, *121*, 6378–6399. https://doi.org/10.1002/2015JA022324

Xu, S., Mitchell, D., Luhmann, J., Ma, Y., Fang, X., Harada, Y., et al. (2017). High-altitude closed magnetic loops at Mars observed by MAVEN. *Geophysical Research Letters*, *44*, 11,229–11,238. https://doi.org/10.1002/2017GL075831

Yeroshenko, Y., Riedler, W., Schwingenschuh, K., Luhmann, J. G., Ong, M., & Russell, C. T. (1990). The magnetotail of Mars: Phobos observation. *Geophysical Research Letters*, *17*, 885–888. https://doi.org/10.1029/GL017i006p00885

Zhang, T. L., Baumjohann, W., Du, J., Nakamura, R., Jarvinen, R., Kallio, E., et al. (2010). Hemispheric asymmetry of the magnetic field wrapping pattern in the Venusian magnetic tail. *Geophysical Research Letters*, *37*, L14202. https://doi.org/10.1029/2010GL044020.2010